American Journal of Electrical and Computer Engineering
2022; 6(1): 15-23
http://www.sciencepublishinggroup.com/j/ajece
doi: 10.11648/j.ajece.20220601.12
ISSN: 2640-0480 (Print); ISSN: 2640-0502 (Online)

Performance of Non-Line of Sight Underwater Optical Wireless Communication Links with Spatial Diversity

Al-Amin Barambu Umar*, Mark Stephen Leeson

School of Engineering, University of Warwick, Coventry, UK

Email address:
A.umar@warwick.ac.uk (Al-Amin B. U.)

*Corresponding author

To cite this article:
Al-Amin Barambu Umar, Mark Stephen Leeson. Performance of Non-Line of Sight Underwater Optical Wireless Communication Links with Spatial Diversity. *American Journal of Electrical and Computer Engineering*. Vol. 6, No. 1, 2022, pp. 15-23.
doi: 10.11648/j.ajece.20220601.12

Received: March 21, 2021; **Accepted**: June 2, 2021; **Published**: February 5, 2022

Abstract: Line-of-sight (LOS) underwater optical wireless communication (UOWC) transmission may suffer blocking and are not always possible due to obstructions from sea creatures, bubbles, large suspended particles and features of the seabed, especially in coastal and turbid water environments. Thus, we present the performance of a spatially diverse non-line-of-sight (NLOS) UOWC system employing continuous phase modulation (CPM), which is shown to offer sensitivity benefits of several dBs over on–off keying (OOK) without coherent reception. We obtain the channel impulse response (CIR) by using Monte Carlo simulation, including absorption and multiple scattering. Turbulence is included by conditioning the CIR on log-normal statistics. To mitigate the resultant fading, we exploit spatial diversity with equal gain combining at the receiver side. Photon counting at the receiver is employed to accommodate shot noise. We compare the saddlepoint and Gaussian approximations for bit error rate (BER) calculations, using the latter for later calculations as it delivers excellent results and is simpler. Our results show that spatial diversity offers performance improvements, for example an 8 dB sensitivity gain at 10^{-9} BER using 1 Gbps 3×1 multiple-input single-output (MISO) transmission over a 20 m link with 0.16 log-amplitude variance. We determine using an upper bound that Intersymbol Interference (ISI) has a significant impact at high bit rates, producing error floors for multiple-output arrangements.

Keywords: Underwater Optical Wireless Communications, Non-line of Sight Link, Multiple Input-multiple Output, Monte Carlo, Turbulence, Bit Error Rate

1. Introduction

The present stage of technological development serving a world population in excess of 7 billion makes significant demands on both non-living (abiotic) and living (biotic) natural resources that is likely to continue into the future [1]. Thus, given the scarcity and resource depletion on dry land, seeking and exploiting undersea sources of supply have become the norm for minerals [2] and food [3]. Such activities typically require submersibles, known as Remotely Operated Vehicles (ROVs), that use an electrical or optical fibre tether cable for communications and control. Despite the reliability and high data speeds of such systems, they are costly to manufacture and operate with limited operating ranges from a surface ship. The relocation of the surface control vehicle to operate in a new region is a very costly prospect [4]. Furthermore, tethered systems are difficult to operate in coastal waters, which are cluttered and dynamic with a risk of entanglement by underwater objects, constraining the paths that may be followed by the ROV [5], leading to the need to calculate paths. Moreover, maintenance costs may also be high due to damage by large marine animals. Thus, there is considerable advantage in the development of reliable broadband wireless communication systems that permit the operation of production and ocean exploration devices. However, radio frequency (RF) waves can only propagate a few metres in seawater using frequencies from 30-300Hz [6], which means that the established technology for underwater communications is based upon acoustic waves [7]. Although these can travel great distances (of the order of km), they offer only low data rates (≤kbps) and suffer from severe communication delays

due to the slow propagation of sound waves in water [6]. Acoustic transceivers are also generally costly, bulky, power-hungry and potentially harmful to marine life [8, 9]. In recent years, the idea of underwater optical wireless communication (UOWC) has emerged as a complementary or alternative solution to underwater acoustic communications [10]. In addition to superior energy efficiency, UOWC offers high throughput and data rates (Gbps), superior security (due to the directivity of the optical signals) and much lower latency (because of the propagation speed of light) than acoustic communications [11, 12].

Underwater, absorption and multiple scattering are the two main factors that induce power loss and degrade the performance of UOWC systems [13]. Thus, a considerable amount of effort in prior work has gone into channel absorption and scattering effects. The channel free fading impulse response has been modelled and simulated using the Monte Carlo (MC) method in [6]-[9]. It is well established that seawater has the lowest attenuation in blue and green light (i.e. transmission wavelength window of 450-550nm), which has emerged as the basis for the development of UOWC [4].

Optical turbulence is another impairment which has a significant impact on the performance of UOWC systems. This results from random variations in the refractive index in water arising from ocean temperature and salinity fluctuations leading fading or received intensity fluctuations, hence degrading UOWC system performance [14]. This contrasts with acoustic links, where multipath reflections are the major source of fading [6]. The study of the impact of turbulence on UOWC systems has received relatively little attention compared to turbulence-induced fading in free space optical communications, where the results of many valuable studies on fading characterization and mitigation have been reported [15]. However, this has begun to change recently with the study of the statistical properties of a gaussian beam travelling through turbulent water [16, 17] Furthermore, the Rytov method has been used to determine the scintillation index of plane and spherical optical wave propagating in the turbulent underwater medium [18]. Vali *et al.* [19] used MC simulation to model UOWC turbulence. They successfully reproduced the lognormal probability density function (PDF) of the received intensity in weak and moderate oceanic turbulence, and their results were in accordance with previous experimental studies.

One of the favourable solutions to resolve the turbulence problem in UOWC is spatial diversity, often using multiple-input-multiple-output (MIMO) transmission and extensively studied in visible light and optical fibre communications [20-22]. MIMO offers spatial diversity gain and performance improvements compared with employing single-input single-output (SISO) transmission. The performance of MIMO-UOWC has been investigated by Jamali and Salehi [23], whose simulation results showed that MIMO can enhance the communication range and alleviate the turbulence-induced fading of the channel. Previously, Simpson [24] used two light emitting diode (LED) transmitters and two pin photodiode receivers to obtain the advantage of spatial diversity in UOWC. However, to the best of our knowledge, all previous spatial diversity work has utilized line-of-sight (LOS) links for the UOWC channel.

So, in this work we use a non-line-of-sight (NLOS) link and take all the channel impairments (absorption, scattering and turbulence) into account. We investigate the performance of spatial diversity employing continuous phase modulation (CPM). We assume an equal gain combiner (EGC) at the receiver side and evaluate the BER performance using the Gaussian approximation (GA) and the saddlepoint approximation (SPA) [25]. We also employ a photon-counting approach to include the impact of shot noise. We obtain the channel free-fading impulse response using MC simulation by taking absorption and scattering into account. This is multiplied by the square of a fading coefficient modelled as a lognormal random variable for oceanic turbulence.

The remainder of this work is organized as follows. Section II describes channel modelling employed, including the fading induced by turbulence. Section III presents the principles of our proposed MIMO UOWC system, including a description of CPM. Section IV introduces the BER expressions with EGC at the receiver. In Section V, we present the results for various system configurations followed by a discussion of the performance. Finally, Section VI concludes the paper.

2. Channel Modelling

We now describe the model of the NLOS underwater channel used. This includes the underwater impairments of absorption, scattering and turbulence.

2.1. Absorption and Scattering

The interaction between a photon and a water particle in the propagation of the optical beam under the water induces either absorption or scattering. The former causes the translation of photon energy into other forms such as thermal energy, which is irreversible. The latter deflects the photon's direction of travel, which also appears as a transmission energy loss because receiver has a finite sized aperture that will capture fewer photons. The extinction (attenuation) coefficient $c(\lambda)$ describes the total loss of energy; it is the sum of the absorption coefficient $a(\lambda)$ and the scattering coefficient $b(\lambda)$ i.e. $c(\lambda) = a(\lambda) + b(\lambda)$. There is considerable variation in $a(\lambda)$ and $b(\lambda)$ (hence in $c(\lambda)$) with water types and source wavelength [3]. As mentioned in the introduction, it has been shown in the literature that absorption and scattering have the lowest impact in the blue-green wavelength interval $450nm \leq \lambda \leq 550nm$ and therefore UOWC systems apply this region of the visible light spectrum for data communications [10].

In this paper, we denote the free fading impulse response between the ith transmitter (Tx) in the system and the jth receiver (Rx) by $h_{0,ij}(t)$. This is found by using MC simulation including both absorption and scattering in the NLOS UOWC link similar to our previous work [26]. To

derive the scattering coefficient, the volume scattering function (VSF) is needed. This describes the angular distribution of light scattered by a suspension of particles at a given wavelength, making use of a phase function [27]. There are several choices for this but here we employ the Fournier-Forand function that provides better performance compared to the more common Henyey-Greenstein (HG) and two-term HG functions [26].

2.2. Turbulence

The most commonly occurring natural examples of optical turbulence are the Earth's atmosphere and the ocean. The physical mechanism of underwater optical turbulence is similar to that of atmospheric optical turbulence since both are mainly caused by the random fluctuations of pressure and temperature of the medium. Description of the absorption and scattering factors was presented in the previous subsection. To capture the turbulence effects, the free fading impulse response $h_{0,ij}(t)$ is multiplied by the square of a fading coefficient ${\alpha^2}_{ij}$ with a log-normal distribution for oceanic weak turbulence [28]. To model the fading presented by turbulence, we let $\alpha = \exp(X)$ so that this has a log-normal fading probability density function (PDF) [28]:

$$f(\alpha) = \frac{1}{\alpha\sqrt{2\pi\sigma_X^2}} \exp\left(-\frac{(\ln(\alpha)-\mu_X)^2}{2\sigma_X^2}\right) \quad (1)$$

Thus, μ_X and σ_X^2 are the mean and variance of the Gaussian distributed fading log-amplitude$X$. Normalizing the fading amplitude ensures that the fading does not attenuate or amplify the average power, i.e. $E[\alpha^2] = 1$ implying that $\mu_X = -\sigma_X^2$ [28].

Therefore, to describe the fading statistics we need to determine the relationship this variance to the turbulence parameters of the ocean. The scintillation index of a light wave with instantaneous point intensity, I, is denoted by σ_I^2 and defined by Korotkova *et al.* [29] as:

$$\sigma_I^2 = \frac{\langle I^2\rangle - \langle I\rangle^2}{\langle I\rangle^2} \quad (2)$$

The scintillation index of light in the turbulent underwater medium can be expressed using the Rytov approximation as [30]:

$$\sigma_I^2 = \exp\left[\frac{0.49\sigma_r^2}{\left(1+1.11\sigma_r^{12/5}\right)^{\frac{7}{6}}} + \frac{0.51\sigma_r^2}{\left(1+0.69\sigma_r^{12/5}\right)^{\frac{5}{6}}}\right] - 1. \quad (3)$$

In (3), σ_r^2 is the Rytov variance [27]:

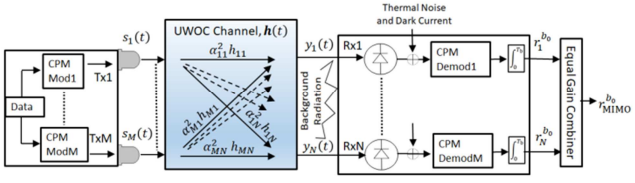

Figure 1. *Proposed Architecture of NLOS-MIMO-UOWC System.*

$$\sigma_r^2 = 37.3K(2\pi/\lambda)^{7/6}L^{11/6} \quad (4)$$

where L is the migration length of the light beam and K is a constant that determines the strength of the turbulence [31]. The value of K ranges from 10^{-14} to $10^{-8}\mathrm{m}^{-2/3}$ which is several orders of magnitude greater than the values of the corresponding constant in atmospheric optical turbulence [31].

3. System Model

The system considered is based on LEDs, which are more suitable than lasers because their wider divergence angles make alignment less critical in turbid water [4]. Although LEDs historically offered modest bit rates, recent developments have removed this drawback [32].

3.1. MIMO UOWC Model

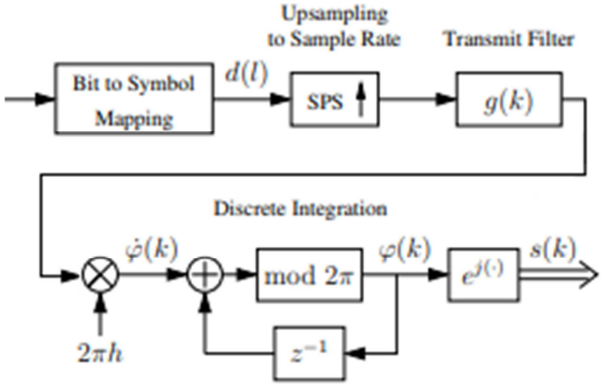

Figure 2. *Discrete CPM modulator.*

We consider a MIMO UOWC system abstracted as in Figure 1, which employs a Tx array of M LEDs that can provide high data rate communications to an array of N Rx photodetectors followed by an equal gain combiner (EGC). The EGC is employed because it has been shown to offer performance close to optimal combining but with considerably reduced complexity [28].

The LEDs are modulated by the electrical inputs after these have been converted to either OOK or the CPM scheme described in Section 3.2. The received optical signal $y(t)$ in a $M \times N$ MIMO system may be described in terms of the transmitted signal $s(t)$ convolved with a $M \times N$ channel impulse response matrix $h(t)$ and multiplied by a matrix $A2(t)$ that contains the squares of the fading coefficients α_{ij} between transmitter i and receiver j, whose amplitude PDF was defined in Section 2.2 above [28]:

$$y(t) = A2(t).h(t) * s(t) \quad (5)$$

This then experiences various sources of noise that must be included in the analysis, namely background optical radiation, dark current and additive white Gaussian noise (AWGN).

3.2. Continuous Phase Modulation (CPM)

The term Continuous-Phase-Modulation (CPM) refers to a

class of coded modulation schemes possessing desirable power and bandwidth efficiency [33]. Although CPM has been shown to achieve near capacity performance in optical communications [34], this has been based on coherent detection with the need for perfect receiver channel state information. When performing hard signal detection at the receiver, CPM also has the advantage that it does not require dynamic thresholding for optimal detection.

CPM presents a constant signal envelope with a continuous phase and constant transmitted carrier power. It is a multi-level scheme and in classical m-ary CPM, a symbol corresponds to $M = \log_2 m$ bits. The discrete CPM modulator shown in Figure 2 produces a signal with symbol duration T described by, for the time interval $lT < t < (l+1)T$, using an arbitrary phase offset φ_0 and instantaneous phase $\varphi(t)$ [35]:

$$s(t) = e^{j(\varphi(t)+\varphi_0)} \tag{6}$$

$$\varphi(t) = 2\pi h \int_0^t \sum_{i=0}^{l} d(i) g(\tau - iT) d\tau \tag{7}$$

where h is the modulation index, $g(t)$ is the transmit filter with the symbols $d(i)$ taken from an M-ary alphabet, where M is even. Figure 2 also shows the process of symbol upsampling by a factor SPS, where $SPS-1$ zeros are inserted between two successive symbols. The transmit filter has a raised cosine impulse response:

$$g(k) = \begin{cases} \frac{1}{2L.SPS}\left(1 - \cos\left(\frac{2\pi k}{L.SPS}\right)\right) & 0 \le k \le L.SPS \\ 0 \; otherwise \end{cases} \tag{8}$$

L is the length of the impulse response in symbol intervals. Using $L = 1$ produces full response CPM, whereas using $L > 1$ results in a partial response, where intersymbol interference (ISI) is introduced for increased spectral efficiency [35]. The response $g(k)$ also fulfils the normalization condition:

$$\sum_{k=0}^{L.SPS} g(k) = \frac{1}{2} \tag{9}$$

4. Photon-Counting BER Analysis

In this section, we express the system BER analytically using a photon-counting method and then applying either the GA or the SPA. Assuming OOK signalling, each bit '1' (ON-state) will be transmitted with a pulse shape $P(t)$ and it is off when sending data bit '0'. For simplicity, we consider the case when $P(t)$ can be expressed as in terms of a unit rectangular pulse $\prod(t)$ in the interval [-1/2, 1/2] and the bit duration time T_b as $P(t) = \prod(\{t - 0.5T_\mathrm{b}\}/T_\mathrm{b})$. Hence, the transmitted signal can be expressed as:

$$S(t) = \sum_{k=-\infty}^{\infty} b_k P(t - kT_\mathrm{b}) \tag{10}$$

for bit $b_k \in \{0,1\}$ in the kth time slot. In the case of SISO, we denote the free-fading impulse response by $h_0(t)$ and the fading coefficient by α. Therefore, after propagating through the channel, the received optical SISO signal becomes:

$$y(t) = S(t) * \alpha^2 h_0(t) = \alpha^2 \sum_{k=-\infty}^{\infty} b_k \Gamma(t - kT_\mathrm{b}) \tag{11}$$

where $\Gamma(t) = h_0(t) * P(t)$ and $*$ denotes the convolution operator.

In the case of MIMO, to make a fair comparison with SISO, using M transmitters the total transmitted power for the ON-state is $P = \sum_{i=1}^{M} P_i$, where P_i is the power transmitted by $\mathrm{Tx_i}$. So, the transmitted signal hereon from $\mathrm{Tx_i}$ is:

$$S_i(t) = \sum_{k=-\infty}^{\infty} b_k P_i(t - kT_b) \tag{12}$$

Thus, the received optical signal after the signal passes from $\mathrm{Tx_i}$ through the channel impulse response $\alpha_{ij}^2 h_{0,ij}(t)$ to $\mathrm{Rx_j}$ will be:

$$y_{i,j}(t) = S_i(t) * \alpha_{ij}^2 h_{0,ij}(t)$$

$$= \alpha_{ij}^2 \sum_{k=-\infty}^{\infty} b_k \Gamma_{i,j}(t - kT_b) \tag{13}$$

with $\Gamma_{i,j}(t) = P_i(t) * h_{0,ij}(t)$. The signals transmitted from all the transmitters are captured at the jth receiver each with its channel impulse response i.e. at the j th receiver, the optical signal received will be $y_j(t) = \sum_{i=1}^{M} y_{i,j}(t)$.

Now, the receiver output is given by $U = N + \xi$, [25] in which N is a poisson distributed Random variable (RV) with mean $m^{(b_0)}$ that includes dark current and background radiation for $b_0 \in \{1,0\}$, and ξ is a zero mean Gaussian distributed RV with variance σ^2. The GA probability of error is then [25]:

$$P_e = Q\left(\frac{m^{(1)} - m^{(0)}}{\sqrt{m^{(1)}+\sigma^2} + \sqrt{m^{(0)}+\sigma^2}}\right) \tag{14}$$

where $Q(x) = \left(1/\sqrt{2\pi}\right) \int_x^\infty \exp(-y^2/2)\, dy$ is the Gaussian Q-function.

The system BER established using the SPA can be expressed as [25]:

$$P_e = \frac{1}{2}[q_+(\beta) + q_-(\beta)] \tag{15}$$

where $q_+(\beta)$ and $q_-(\beta)$ are the error probabilities when binary "0" and "1" are sent respectively, namely that the photoelectron count at the output of the receiver, z, fulfils:

$$q_+(\beta) = Pr(z > \beta | \text{zero}) \approx \frac{\exp[\phi_0(s_0)]}{\sqrt{2\pi\phi_0''(s_0)}} \tag{16}$$

$$q_-(\beta) = Pr(z \le \beta | \text{one}) \approx \frac{\exp[\phi_1(s_1)]}{\sqrt{2\pi\phi_1''(s_1)}} \tag{17}$$

$$\phi_{b_\mathrm{i}}(s) = \ln\left[\psi_{z(b_\mathrm{i})}(s)\right] - s\beta - \ln|s| \tag{18}$$

where $b_\mathrm{i} = 0,1$ and $\psi_{z(b_\mathrm{i})}(s)$ is the moment generating function (MGF) of the receiver output when binary value b_i is sent. Moreover, s_0 is the positive, real root of $\phi_0'(s)$ and s_1 is the negative, real root of $\phi_1'(s)$. The receiver optimum threshold β is chosen so that it reduces the probability of error (i.e. $P_{be}/d\beta = 0$).

We now present the required expressions for both the GA

and SPA for the different link configurations when EGC is used.

4.1. SISO UOWC Link

From the previous section, the received SISO photodetected signal can be expressed as:

$$r_{SISO}^{b_0} = y_{SISO}^{(b_0)} + v_{th} \tag{19}$$

Here, $y_{SISO}^{(b_0)}$ is a Poisson distributed RV with mean $m^{(b_0)}$, conditioned on α and $\{b_k\}_{k=-L}^{0}$, that is given by [31]:

$$m^{(b_0)} = \frac{\eta\alpha^2}{hf}\{\sum_{k=-L}^{0} b_k \Gamma_k^{\text{Int}}\} + (\gamma_b + \gamma_d)T_b \tag{20}$$

$$\Gamma_k^{\text{Int}} = \int_0^{T_b} \Gamma(t - kT_b)dt \tag{21}$$

where $\eta, f, h,$ and L are the quantum efficiency, Planck's constant, carrier frequency of the optical source and channel memory, respectively. The mean count rates of the Poisson distributed dark current noise and background radiation are γ_d and γ_b, respectively.

The other noise contribution, v_{th} is a zero mean Gaussian distributed RV corresponding to the integrated thermal noise with variance σ_{th}^2, given by:

$$\sigma_{th}^2 = \frac{2k_b T_b T_r}{R_L q^2} \tag{22}$$

where k_b, T_r, R_L, q are Boltzmann's constant, receiver equivalent temperature, load resistance and the electronic charge respectively.

The receiver output MGF conditioned on α is given below [28]:

$$\psi_{z\ \ {}_{SISO}^{(b_0)}|\alpha}(s) = M_{\text{T}}(s) M_{\text{SISO}}(s) M_{\text{SISO-ISI}}(s) \tag{23}$$

$$M_{\text{SISO}}(s) = \exp\left(\left[\gamma_{SISO}^{(bd)} + \alpha^2 b_0 \gamma^{(0)}\right]E(s)\right) \tag{24}$$

$$M_{\text{T}}(s) = \exp\left(\frac{s^2\sigma_{th}^2}{2}\right) \tag{25}$$

$$M_{\text{SISO-ISI}}(s) = \prod_{k=-L}^{-1}\left[\frac{1+\exp\{\alpha^2\gamma^{(k)}E(s)\}}{2}\right] \tag{26}$$

where $E(s) = e^s - 1, \gamma_{SISO}^{(bd)} = (\gamma_b + \gamma_d)T_b$ and $\gamma^{(k)} = \frac{\eta}{hf}\int_{-kT_b}^{-(k-1)T_b} \Gamma(t)dt$.

In physical terms, $\gamma^{(k\neq 0)}$ indicates the effect of ISI and $\gamma^{(k=0)}$ illustrates the desired signal contribution (i.e. $\gamma^{(k=0)} = \gamma^{(s)}$). This MGF can be utilized in the SPA equation (18) or to find the appropriate variance for the GA, both conditioned on α. Thus, we can obtain into the conditional BER $P_{e|\alpha}$and by averaging over the fading coefficient α, the final BER:

$$P_e = E_\alpha\left[P_{e|\alpha}\right] = \int P_{e|\alpha}\, f_\alpha(\alpha)d\alpha \tag{27}$$

4.2. MIMO UOWC Link

Each of the *N* receiving apertures receives the sum of all transmitted signals, which then are photodetected and experience noise. Hence, at the jth receiver, the photo-detected signal can be expressed as:

$$r_j^{b_0} = y_j^{b_0} + v_{th,j} \tag{28}$$

In this case, $y^{(b_0)}$ is a Poisson distributed RV with mean $m_j^{(b_0)}$, conditioned on $\{\alpha\}_{i=1}^{M}$ and $\{b_k\}_{k=-L_{ij}}^{0}$, thus [28]:

$$m_j^{(b_0)} = \frac{\eta}{hf}\sum_{i=1}^{M}\{\sum_{k=-Lij}^{0} \alpha_{ij}^2 b_k \Gamma_{i,j}^{\text{Int}}\} + \left(\gamma_{b\,j} + \gamma_{dj}\right)T_b \tag{29}$$

$$\Gamma_{i,j}^{\text{Int}} = \int_0^{T_b} \Gamma_{i,j}(t - kT_b)dt \tag{30}$$

The mean count rates of the Poisson distributed dark current noise and background radiation at the jth Rx are $\gamma_{d\,j}$ and $\gamma_{b\,j}$, respectively; L_{ij} is the channel memory between TX_i and RX_j.

Once again, the other noise contribution, $v_{th,j}$ is a zero mean Gaussian distributed RV with variance $\sigma_{th,j}^2 = \sigma_{th}^2$, which is equivalent to the combined thermal noise of the jth Rx.

The MIMO output MGF is then, conditioned on the fading coefficient vector $\vec{\alpha}$, [28]:

$$\psi_{r(b_0),MIMO|\vec{\alpha}}(s) = M_{\text{T}}(\sqrt{N}s) M_{\text{MIMO}}(s) \prod_{j=1}^{N} M_{\text{MIMO-ISI}}(s) \tag{31}$$

$$M_{\text{MIMO}}(s) = \exp\left(\left[\gamma_{MIMO}^{(bd)} + X_{\text{MIMO}}\right]E(s)\right) \tag{32}$$

$$X_{\text{MIMO}} = \sum_{j=1}^{N}\sum_{i=1}^{M} b_0 A_{ij}^{(0)} \tag{33}$$

$$M_{\text{MIMO-ISI}}(s) = \prod_{k=-L_{\max}}^{-1}\frac{1}{2}\left[1 + \prod_{i=1}^{M}\exp\left(A_{ij}^{(k)}E(s)\right)\right] \tag{34}$$

$$A_{ij}^{(k)} = \alpha_{ij}^2 \gamma_{i,j}^{(k)} \tag{35}$$

where $\gamma_{i,j}^{(k)} = \frac{\eta}{hf}\int_{-kT_b}^{(-k+1)T_b} \Gamma_{i,j}(t)dt$, $\gamma_{MIMO}^{(bd)} = (\gamma_b + N\gamma_d)T_b$ and $L_{\max} = \max\{L_{11}, L_{12}, \ldots L_{MN}\}$.

For the SIMO and MISO schemes, the output MGFs can be easily found by substituting $M = 1$ and $N = 1$ respectively in (31-35). In a similar way to SISO, the conditional BER results from inserting (31-35) into (16-18) and the final BER from averaging over fading coefficients $\vec{\alpha}$ similarly to (27).

For the GA conditioned on $\vec{\alpha}$ and b_k, the zero mean Gaussian RV has variance $N\sigma_{th}^2$ while the Poisson RV has mean and variance $m^{(b_0)}$ given by [31]:

$$m_{MIMO}^{b_0} = \gamma_{MIMO}^{(bd)} + \sum_{j=1}^{N}\sum_{i=1}^{M}\left[\tau_{i,j}^{(b_0)}\alpha_{ij}^2\right] \tag{36}$$

where $\tau_{i,j}^{(b_0)} = b_0\gamma_{i,j}^{(s)} + \sum_{k=-Lij}^{-1} b_k \gamma_{i,j}^{(k)}$ conditioned on $\{b_k\}_{k=-L_{ij}}^{0}$.

Then, the average BER of the system becomes:

$$P_e \approx Q\left(\frac{m_{MIMO}^{(1)} - m_{MIMO}^{(0)}}{\sqrt{m_{MIMO}^{(1)} + N\sigma_{th}^2} + \sqrt{m_{MIMO}^{(0)} + N\sigma_{th}^2}}\right) \tag{37}$$

4.3. Upper BER Bound for ISI

To deal totally comprehensively with ISI would require consideration of an infinite stream of previous bits that could influence the current bit. Since, the effects of ISI on the current bit are reduced as the previous bits become further in the past, a truncation of the number of bits is employed as captured here by L and $L_{\max}$ in (26) and (34) respectively.

In addition, methods based on the expectation on the values of previous bits may also be employed [39], which can utilize the GA [40]. Here, we use a particular bit sequence to produce an upper bound, which is known to be effective for UOWC [28]. When transmitting a zero, i.e. $b_0 = 0$, we take $b_{k\neq 0} = 1$ and when transmitting a one, i.e. $b_0 = 1$, we take $b_{k\neq 0} = 0$. These conditions ensure that for a zero, there is maximum chance that ISI will cause an excessive count that exceeds the decision threshold and for a one, there is no addition to the pulse size from ISI.

5. Results and Discussion

We now present the numerical results for the BER of various NLOS UOWC system scenarios. A log-normal distribution has been considered for the fading statistics with the same log-amplitude variance for all of the links, the transmitters employ equal power of P/M and the receivers have equal aperture areas of A/N, where A is the SISO aperture area. We simulated the turbulence free fading impulse response via MC simulation in coastal water with the parameters shown in Table 1 since this was the most likely environment for NLOS applications. Table 1 also shows the key noise parameters that affect the received signal. Background radiation had a negligible effect in our system given the significant attenuation of sunlight at likely orating depths. Based on further values in [37, 38], the noise characteristics were $\gamma_b \approx 1.8094 \times 10^8 \mathrm{s}^{-1}$, $\gamma_d \approx 76.625 \times 10^8 \mathrm{s}^{-1}$, and $\sigma_{th}^2/T_b = 3.12 \times 10^{15} \mathrm{s}^{-1}$.

Table 1. *Channel parameters from [36-38].*

Parameter	Symbol	Value
Coastal water absorption coefficient	a	0.179 m^{-1}
Coastal water scattering coefficient	b	0.219 m^{-1}
Coastal water attenuation coefficient	c	0.398 m^{-1}
Receiver half angle FOV	θ_{FOV}	40^0
Aperture diameter	D_0	20 cm
Source wavelength	λ	532 nm
Refractive index of coastal water	n	1.331
Transmitter beam divergence	θ_{div}	0.02^0
Rx photon weight threshold	w_{th}	10^{-6}
Sample time		0.01 s
Optical filter bandwidth	$\Delta\lambda$	10 nm
Optical filter transmissivity	T_F	0.8
Quantum efficiency	η	0.8
Load resistance	R_{L}	100 Ω
Dark Current	I_{dc}	1.226 nA
Equivalent temperature	T_{e}	290K
Channel memory	$L_{\max}$	3

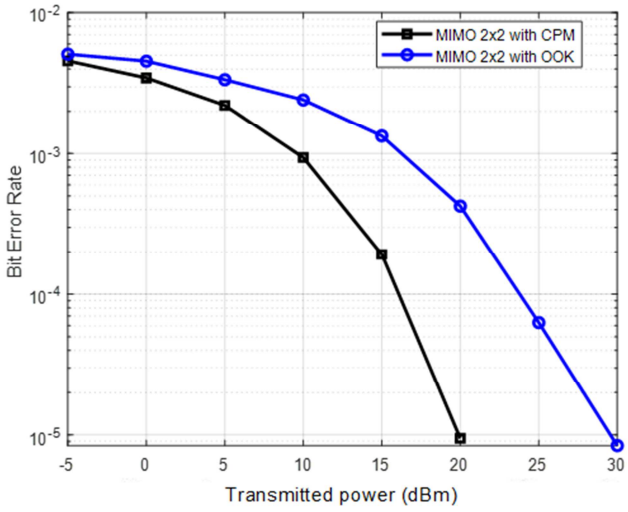

Figure 3. *Comparison of BER for OOK and CPM.*

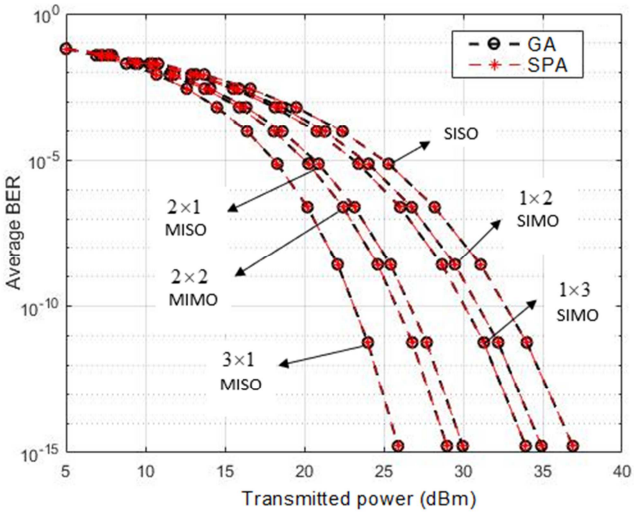

Figure 4. *Comparison of GA and SPA.*

The proposed scheme was simulated in MATLAB using Lambertian LED sources located at (y, z) coordinates $(\pm 2.5\ \mathrm{m}, \pm 2.5\ \mathrm{m})$, taking x as the propagation direction. We first compared OOK and CPM (using $l = 4$) in a 2x2 MIMO 1 Gbps NLOS configuration by simulation through 20 m of coastal water using $\sigma_X = 0.4$ to compare the performance of both modulation schemes. As can be seen from the results in Figure 3, CPM was superior to OOK, at a BER of 10^{-4} CPM offered an advantage in excess of 7 dB over OOK that rises to some 10 dB at 10^{-5}. Thus, CPM was taken as the modulation scheme for the rest of what follows.

Next, we compared the results obtained using the GA and SPA, to ascertain which should be employed. Figure 4 shows the results for a range of configurations using the same parameters as in Figure 3 with the photon counting approach rather than simulation. It can be observed that the results from the GA and SPA are in excellent agreement, meaning that the from can be employed here without the need for the extra computation entailed in the latter. Hence, the GA was employed to obtain the remaining results that follow.

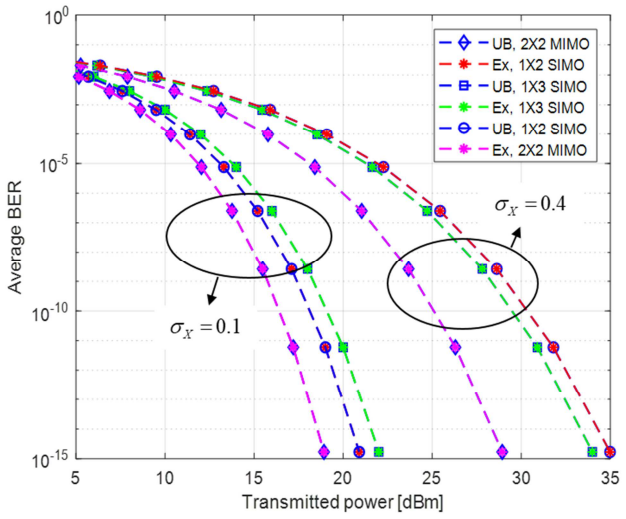

Figure 5. *Exact (Ex) and Upper bound (UB) BER at 1 Gbps in a 20 m coastal water link for various configurations.*

Figure 5 shows the results of employing the GA to evaluate the upper bound and exact BER of the system with various configurations (2×2 MIMO, 1×2 SIMO, and 1×3 SIMO) at a 1 Gbps transmission rate in 20 m of coastal water. We consider two regimes, namely the moderately strong turbulent channel with $\sigma_X = 0.4$ used previously and a weakly turbulent channel having $\sigma_X = 0.1$. There is an excellent match between the exact and upper bound BER curves, which are tight in all configurations. In the $\sigma_X = 0.4$ regime, the 1×3 SIMO configuration gives better performance than 1×2 SIMO at high SNRs, where fading has a more degrading effect than ISI and absorption. This is understandable because each Rx in 1×3 SIMO has reduced aperture area but higher dark current and thermal noise than 1×2 SIMO. In the weaker regime of $\sigma_X = 0.1$, fading has a negligible effect on the system BER and absorption; scattering including noise has the more dominant effect. Hence, for low SNRs 1×2 SIMO provides better performance than 1×3 SIMO. Realistically, since the underwater channel suffers notably from turbulence, 1×3 SIMO offers greater fading mitigation as well as compensating for the effects of excess noise and smaller receiver apertures area since it benefits from one more independent link than 1×2 SIMO. Nevertheless, 2×2 MIMO has the same receiver aperture area as 1×2 SIMO but gives better performance in all regimes as it benefits from independent links. It is clear that Tx diversity yields better results than Rx diversity because of the effects of aperture size and noise power.

In Figure 6, we investigate the effect of ISI on the performance of the system for various configurations. The figure depicts the upper bound BER results with $\sigma_X = 0.4$ in coastal water for different configurations (SISO, 2×1MISO, 1×2 SIMO, 3×1 MISO, 1×3 SIMO and 2×2 MIMO) using a typical NLOS data rate of 0.3 Gbps and a significantly higher data rate of 30 Gbps. At the lower data rate, significant improvements in system.

At the lower data rate, 10^{-9} sensitivity improvements over SISO are seen for all diversity configurations. These range from 2.7 dB for 1×2 SIMO to 9.3 dB using 3×1 MISO. Thus, transmitter diversity is superior to receiver diversity; in the MISO structure all the transmitters are pointed at one receiver which means that the photons received by this single receiver experience less scattering. However, in the SIMO configuration, the transmitter source points more towards one of the detectors and then photons that experience relatively high scattering are captured by the other receivers through indirect paths causing ISI. The use of MIMO does produce a further (albeit reduced) benefit, for example 2×1 MISO offers an improvement of 6.8 dB and 2×2 MIMO 7.7 dB. It is also apparent that increasing the data rate significantly impacts the system performance of some configurations via ISI. All the receiver diversity schemes (1×2 SIMO, 1×3 SIMO and 2×2 MIMO) exhibit error floors at 30 Gbps. Transmitter diversity fares much better, with 2×1MISO and 3×1 MISO delivering 10^{-9} sensitivity improvements of 8.4 dB and 11.6 dB, respectively.

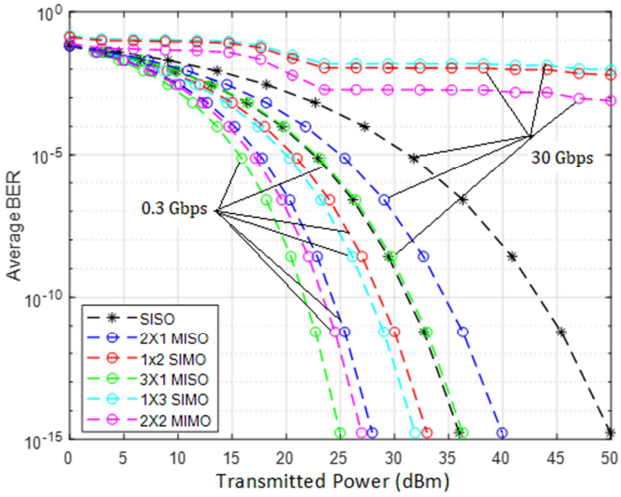

Figure 6. *Effect of ISI on 20 m coastal water link for various configurations at 0.3 Gbps and 30 Gbps.*

6. Conclusion

In this work, the performance of MIMO NLOS UOWC employing EGC at the receiver side has been studied. The effects of absorption, scattering and turbulence were all taken into account. The NLOS channel impulse response in the absence of fading was obtained using MC numerical simulations and turbulence effect was included as a multiplicative fading coefficient. CPM modulation was shown to give better BER results than OOK because of its higher spectral efficiency. We evaluated the system BER performance using a photon counting approach with spatial diversity. We investigated the GA and SPA to produce the final results and both gave very similar results for the BER. Thus, the GA was adopted for later calculations since it was computationally simpler and so faster, which was of great benefit once the configurations increased in complexity. Coastal waters are the most likely environment for NLOS systems, given the preponderance of clutter close to land. We thus determined the BER for these waters, where we saw 10^{-9}

sensitivity gains of up to 8 dB using MISO using a 1 Gbps data rate over a 20 m link with 0.16 log-amplitude variance; with SIMO was less beneficial and there was a small gain over MISO by using MIMO. We adopted an established tight upper bound for determining the impact of ISI. In the same water conditions, using a high bit rate of 30 Gbps showed the effects of ISI. Whilst MISO still delivered benefits of up to 11.6 dB, SIMO and MIMO developed error floors, preventing low BER values. Thus, multiple transmitter schemes are highly recommended in NLOS coastal transmission to improve the achievable bit rates. Our numerical results have shown that spatial diversity can compensate the ISI effects by mitigating the fading effects and possibly extend communication ranges. Further work will be required for experimental demonstration and hybrid acoustic-optical links.

Acknowledgements

Al-Amin Umar Barambu is supported by the facilities in the School of Engineering, University of Warwick, UK.

References

[1] Livi Bacci, M.: 'A Concise History of World Population' (Wiley, 6th edn. 2017).

[2] Petersen, S., Krätschell, A., Augustin, N., Jamieson J., Hein, J. R., Hannington, M. D.: 'News from the seabed – Geological characteristics and resource potential of deep-sea mineral resources', Marine Policy, 2016, 70, pp. 175-187.

[3] Chen, O, L.: 'The big picture: future global seafood markets', in Cisneros-Montemayor, A. M., Cheung, W. W. L, Ota, Y. (Eds.): 'Predicting Future Oceans: Sustainability of Ocean and Human Systems Amidst Global Environmental Change' (Elsevier, 2019 1st edn.), pp. 241-248.

[4] Zeng, Z., Fu, S., Zhang, H., Dong, Y., Cheng, J.: 'A survey of underwater optical wireless communications', IEEE Communications Surveys and Tutorials, 2017, 19 (1), pp. 204-238.

[5] McCammon, S., Hollinger, G. A.: 'Planning and executing optimal non-entangling paths for tethered underwater vehicles', Proc. IEEE International Conference on Robotics and Automation (ICRA), Singapore, May 2017, pp. 3040-3046.

[6] Pompili, D., Akyildiz, I. F.: 'Overview of networking protocols for underwater wireless communications', IEEE Comm. Mag., 2009, 47, (1), pp. 97–102.

[7] Song, A., Stojanovic, M., Chitre, M.: 'Editorial Underwater Acoustic Communications: Where we stand and what is next?', IEEE Journal of Oceanic Engineering, 2019, 44, (1), pp. 1–6.

[8] Partan, J., Kurose, J., Levine, B. N.: 'A survey of practical issues in underwater networks', ACM SIGMOBILE Mobile Comput. Comm. Rev., 2007, 11, (4), pp. 23–33.

[9] Au, W. W., Nachtigall, P. E., Pawloski, J. L.: 'Acoustic effects of the ATOC signal (75 Hz, 195 dB) on dolphins and whales', J. Acoust. Soc. Amer., 1997, 101, (5), pp. 2973–2977.

[10] L. J. Johnson, F. Jasman, R. J. Green, M. S. Leeson: 'Recent Advances in Underwater Optical Wireless Communication', Underwater Technology, 2014, 32, (3), pp. 167-175.

[11] Akhoundi, F., Jamali, M. V., Banihassan, N., Beyranvand, H., Minoofar, A., Salehi, J. A.: 'Cellular underwater wireless optical CDMA network: potentials and challenges', IEEE Access, 2016, 4, pp. 4254–4268.

[12] Saeed, N. Celik, A., Al-Naffouri, T., Alouini, M.-S.: 'Underwater Optical Wireless Communications, Networking, and Localization: A Survey', Ad Hoc Networks, 2019, 94, art. 101935.

[13] Cox, W., Muth, J.: 'Simulating channel losses in an underwater optical communication system', J. Opt. Soc. Am. A, 2014, 31, (5), pp. 920-934.

[14] Tang, S., Zhang, X., Dong, Y.: 'Temporal statistics of irradiance in moving turbulent ocean', Proc. IEEE OCEANS, Bergen, Norway, June 2013, pp. 1–4.

[15] Kaushal, H., Kaddoum, G.: 'Optical Communication in Space: Challenges and Mitigation Techniques', IEEE Communications Surveys & Tutorials, 2017, 19, (1), pp. 57-96.

[16] Korotkova O., Farwell N., Shchepakina, E.: 'Light scintillation in oceanic turbulence', Waves in Random and Complex Media, 2012, 22, (2), pp. 260–266.

[17] Farwell, N., Korotkova, O.: 'Intensity and coherence properties of light in oceanic turbulence', Optics Communications, 2012, 285, (6), pp. 872–875.

[18] Ata, Y., Baykal Y.: 'Scintillations of optical plane and spherical waves in underwater turbulence', Journal of the Optical Society of America A, 2014, 31, (7), pp. 1552–1556.

[19] Vali, Z., Gholami, A., Ghassemlooy, Z. et al.: 'Modeling turbulence in underwater wireless optical communications based on Monte Carlo simulation', Journal of the Optical Society of America A, 2017, 34, (7), pp. 1187-1193.

[20] Jansen, S. L, Morita, I., Schenk, T. C., *et al.*: 'Long-haul transmission of 16 × 52.5 Gb/s polarization-division-multiplexed OFDM enabled by MIMO processing', Journal of Optical Networking, 2008, 7, (2), pp. 173–182.

[21] Azhar, A. H., Tran, T., O'Brien, D. C.: 'A Gigabit/s Indoor Wireless Transmission Using MIMO-OFDM Visible-Light Communications', IEEE Photonics Technology Letters, 2013, 25, (2), pp. 171–174.

[22] Hong, Y., Wu, T., Chen, L. K.: 'On the performance of adaptive MIMO-OFDM indoor visible light communications', IEEE Photonics Technology Letters, 2016, 28, (8), pp. 907–910.

[23] Jamali, M. V., Salehi, J. A.: 'On the BER of multiple-input multiple-output underwater wireless optical communication systems', Proc. Optical Wireless Communications (IWOW), Istanbul, Turkey, September 2015, pp. 26–30.

[24] Simpson, J. A.: 'A 1 Mbps underwater communications system using LEDs and photodiodes with signal processing capability', MS thesis, North Carolina State University, Raleigh, 2008.

[25] Einarsson, G.: 'Principles of Lightwave communications' (Wiley, 1996).

[26] Umar, A. B., Leeson, M. S., Abdullahi, I.: 'Modelling Impulse Response for NLOS Underwater Optical Wireless Communications', Proc. IEEE International Conference on Electronics Computer and Computation (ICECCO), Abuja, Nigeria, December 2019, pp. 1-6.

[27] Lee M. E., Korchemkina E. N.: 'Volume Scattering Function of Seawater', in: Kokhanovsky A. (Ed.): 'Light Scattering, Radiative Transfer and Remote Sensing', (Springer, 2018), pp 151-195.

[28] Jamali, M. V., Salehi, J. A., Akhoundi, F.: 'Performance Studies of Underwater Wireless Optical Communication Systems with Spatial Diversity: MIMO Scheme', IEEE Transactions on Communications, 2017, 65, (3), pp. 1176-1192.

[29] Korotkova, O., Farwell, N., Shchepakina, E.: 'Light scintillation in oceanic turbulence', Waves in Random and Complex Media, 20102, 22, (2), pp. 260–266.

[30] Andrews, L. C., Philips, R. L., Hopen, C. Y.: 'Laser Beam Scintillation with Applications', (SPIE, 2001).

[31] Liu, W., Xu, Z., Yang, L.: 'SIMO detection schemes for underwater optical wireless communication under turbulence', Photonics Research, 2015, 3, (3), pp. 48-53.

[32] Bian, R., Tavakkolnia, I., Haas, H.: '10.2 Gb/s Visible Light Communication with Off-the-Shelf LEDs', Proc. European Conference on Optical Communication (ECOC), Rome, Italy, September 2018, pp. 1-3.

[33] Barbieri, A., Fertonani, D., Colavolpe, G.: 'Spectrally-efficient continuous phase modulations', IEEE Transactions on Wireless Communications, 2009, 8, (3), pp. 1564–1572.

[34] Detwiler, T. F., Searcy, S. M., Ralph, S. E., Basch, B.: 'Continuous phase modulation for fiber-optic links', Journal of Lightwave Technology, 2011, 29, (24), pp. 3659–3671.

[35] Weikert, O, Zölzer, U: 'A wireless MIMO CPM system with blind signal separation for incoherent demodulation', Advances in Radio Science, 2008, 6, pp. 101–105.

[36] Umar, A. B., Leeson, M. S.: 'Performance of Non-Line-of-Sight Underwater Optical Wireless Communications; Proc. 2nd IEEE British and Irish Conference on Optics and Photonics (BICOP), London, United Kingdom, December 2019, pp. 1-4.

[37] Jaruwatanadilok, S.: 'Underwater Wireless Optical Communication Channel Modeling and Performance Evaluation using Vector Radiative Transfer Theory', IEEE Journal on Selected Areas in Communications, 2008, 26, (9), pp. 1620-1627.

[38] Giles, J. W., Bankman, I. N.: 'Underwater optical communications systems. Part 2: basic design considerations', Proc. IEEE Military Communications Conference (MILCOM), Atlantic City, NJ, October 2005, pp. 1700-1705.

[39] Leeson, M. S.: 'A Fast Approximation for Bit Error Rate Calculations in Optically Preamplified Receivers', Electron. Lett., 1997, 33, (15), pp. 1329-1330.

[40] El-Howayek, G., Zhang, C., Li, Y., Ng, J. S., David, J. P. R.: 'On the Use of Gaussian Approximation in Analyzing the Performance of Optical Receivers', IEEE Photonics Journal, 2014, 6, (1), pp. 1-8.